Monthly Notices
of the
ROYAL ASTRONOMICAL SOCIETY

MNRAS **430,** 787–796 (2013) doi:10.1093/mnras/sts408

# Chemical reactions induced in frozen formic acid by heavy ion cosmic rays

Diana P. P. Andrade,[1]⋆ Ana L. F. de Barros,[2] Sérgio Pilling,[1] Alicja Domaracka,[3] Hermann Rothard,[3] Philippe Boduch[3] and Enio F. da Silveira[4]

[1]*Inst. of Research and Development, Univ. do Vale do Paraíba, Av. Shishima Hifumi, 2911, CEP 12244−000, São José do Campos, SP, Brazil*
[2]*Departamento de Disciplinas Básicas e Gerais, CEFET-RJ, Av. Maracanã, 229, CEP 20271-110, Rio de Janeiro, RJ, Brazil*
[3]*Centre de Recherche sur les Ions, les Matériaux et la Photonique (CEA/CNRS/ ENSICAEN/Université de Caen-Basse Normandie), CIMAP-CIRIL-Ganil, Boulevard Henri Becquerel, BP 5133, F-14070 Caen Cedex 05, France*
[4]*Dept. de Física, Pontifícia Univ. Católica do Rio de Janeiro, Rua Marquês de São Vicente 225, 22451-900, Rio de Janeiro, RJ, Brazil*

Accepted 2012 November 14. Received 2012 November 8; in original form 2012 May 18

## ABSTRACT

We studied the effects produced by the interaction of heavy ion cosmic rays with interstellar and cometary organic molecules in the solid phase. Formic acid (HCOOH) ice at 15 K was irradiated by 267-MeV $^{56}Fe^{22+}$ ions and the chemical evolution was analysed using Fourier transform infrared spectroscopy. The destruction cross-section of HCOOH and the formation cross-sections of the produced molecular species have been determined; the sputtering yield values are also discussed. The most abundant chemical species formed by Fe ion irradiation are CO, $CO_2$ and $H_2O$. The half-life of frozen formic acid molecules in the interstellar medium, as a result of interaction with the different cosmic ray constituents, is evaluated to be $10^8$ yr, considering that the destruction cross-section $\sigma_d$ of heavy ions is ruled by a power law as a function of the electronic stopping power $S_e$ (i.e. $\sigma_d \sim S_e^{3/2}$). Moreover, a complementary study based on mass spectrometry data from the literature has been performed, in order to understand the HCOOH molecule radiolysis, the desorption of its product and the chemical reaction pathways in ice.

**Key words:** astrochemistry – molecular data – techniques: spectroscopic – methods: laboratory – ISM: molecules – infrared: ISM.

## 1 INTRODUCTION

The analysis of the formation of prebiotic molecules in the astrophysical environment can provide qualitative and quantitative information for a discussion of the first steps related to the origin of life. Star-forming regions have been studied in order to search for a variety of biologically interesting molecules. Among these molecules are formic acid (HCOOH) and acetic acid ($CH_3COOH$), which have common structural elements, such as glycine ($NH_2CH_2COOH$), which is the simplest amino acid. Formic acid and glycine serve as model systems for the properties of larger and more complex amino acids, or even small peptides; it is necessary to understand their behaviour during exposure to high-energy radiation. Their dissociation process and the resulting ionic fragment yields play an essential role in the evolution of interstellar chemistry.

Formic acid has been observed in several astronomical sources, such as comets, protostellar ices, NGC 7538: IRS9, chondritic meteorites, dark molecular clouds and regions associated with stellar formation (Briscoe & Moore 1993; Schutte et al. 1996; Ehrenfreund & Charnley 2000; Ehrenfreund & Schutte 2000; Crovisier et al. 2004). Formic acid has also been observed in some massive star-forming regions, such as Sgr B2, Orion KL and W 51 (Liu et al. 2002). Inside dense molecular clouds, as well as in the protostellar disc and on the surface of Solar system bodies, icy grains are protected from the ultraviolet (UV) photons coming from the central star. Thus, energetic cosmic rays and X-ray photons are the main ionizing particles that are capable of penetrating these regions and inducing the formation of new molecules.

Several experimental and theoretical studies of the dissociation of formic acid have been performed in the gaseous and solid phases, using vacuum ultraviolet (VUV) as the ionizing agent (Leach et al. 2002) and soft X-ray photons (Boechat-Roberty, Pilling & Santos 2005; Guillemin, Stolte & Lindle 2009; Andrade et al. 2009; Pilling et al. 2011a). These also employed low-energy electrons (0.5–2 keV), as well as energetic protons with energies covering the range 0.13–2.0 MeV (Pilling et al. 2006b). In addition, electron-induced decarboxylation in condensed films of formic acid has been studied in the energy range 0.7–20 eV using high-resolution electron energy loss spectroscopy (Martin et al. 2008). The vibrational spectrum of formic acid in the gaseous phase has been measured by infrared (IR; Millikan & Pitzer 1957, 1958; Maréchal 1987) and Raman spectroscopies (Bertie et al. 1986). Formic acid

⋆ E-mail: dianaufrj@gmail.com

in the solid phase has been studied by IR spectroscopy using the matrix-isolation technique (Reva et al. 1994; Maçôas et al. 2003).

There have been recent photolysis studies, using soft X-ray photons (Andrade et al. 2008), and radiolysis studies, using $^{252}$Cf fission fragments (FF), of formic acid at 56 K (see Andrade et al. 2007). These studies show that there are similar effects induced by these two types of radiation on the icy surface. All ionic species produced by the impact of X-ray photons have also been observed after the impact of energetic ions (cosmic ray analogues). However, the opposite is not true. Some species, such as carboxylic anion $COOH^-$ (or $HCOO^-$), are only observed in radiolysis experiments, which indicates that many triggered reaction pathways are different.

The knowledge of the dissociation processes and their ionic fragment yields is relevant to the chemistry of the interstellar medium (ISM) because photodissociation of organic molecules in star-forming regions, comets and other astrophysics environments might lead to the production of large organic molecules. In this way, laboratory data (the formation and destruction cross-sections, and the half-lives for these compounds) combined with astronomical observations can help to elucidate the physicochemical processes occurring in the astronomical sources.

To study the effects produced by the interaction of energetic cosmic rays with condensed (ice-phase) interstellar and cometary organic molecules, we have irradiated HCOOH ices with high-energy Fe ions, a cosmic ray constituent that has been suggested to be highly efficient at inducing chemical reaction in ices (de Barros et al. 2011b). The sputtering yields, the destruction rate of HCOOH and the rate of formation of new molecular species have been determined from recorded spectra. Moreover, a complementary analysis has been conducted with previous results on mass spectrometry using heavy ions as ionizing agents.

## 2 EXPERIMENTAL DETAILS

The experiments, which have simulated the effects of heavy and highly ionized cosmic rays on astrophysical cold surfaces, were carried out at the Grand Accélérateur National d'Ions Lourds (GANIL), Caen, France.

The HCOOH vapour was condensed on a CsI substrate at 13 K and irradiated by 267-MeV $^{56}Fe^{22+}$ (5 MeV $u^{-1}$) ions. An *in situ* analysis was performed using a Fourier transform infrared (FTIR) spectrometer (Nicolet Magna 550) from 4000 to 600 $cm^{-1}$ with a resolution of 1 $cm^{-1}$. The chamber pressure during the experiments was below $2 \times 10^{-8}$ mbar. The spectra were collected at different fluences up to $1 \times 10^{13}$ ions $cm^{-2}$. The Fe flux was about $1 \times 10^9$ ions $cm^{-2}$ $s^{-1}$. Further details have been given elsewhere (Seperuelo Duarte et al. 2009; de Barros et al. 2011b). The sample holding system can be placed in three different positions: gas deposition, FTIR measurement and perpendicular ion irradiation. The sample was purchased commercially from Sigma–Aldrich with purity greater than 99.8 per cent, and it was further degassed through several freeze–pump–thaw cycles, before the vapour was admitted into the chamber. The ice thickness was around 2 μm, which was calculated by using the methodology described by Pilling et al. (2011b).

## 3 RESULTS

Fig. 1 shows the middle-range IR spectra of formic acid before and after irradiation (at final fluence of $1 \times 10^{13}$ ions $cm^{-2}$). From the dependence of the molecular column density of the sample on the fluence, the dissociation cross-sections for a vibration mode and the formation cross-sections, as well as the changes on the structure of the ice, are determined using the IR spectrum.

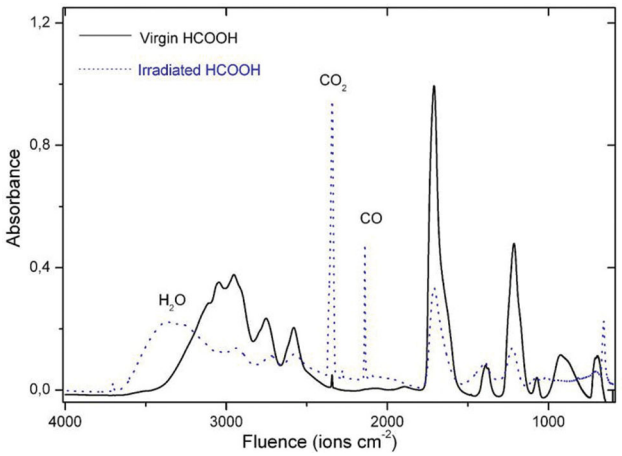


**Figure 1.** Experimental IR spectra of HCOOH ice at 13 K before (solid line) and after (dotted line) irradiation at fluences of $1 \times 10^{13}$ ions $cm^{-2}$ with 267-MeV $^{56}Fe^{22+}$ ions.

**Table 1.** Position of the vibrational bands observed in this work before irradiation and those reported by Cyriac & Pradeep (2005). The symbols $\nu$ and $\delta$ indicate stretching or bending modes, respectively.

| Wavenumber from this work ($cm^{-1}$) | Wavenumber from Cyriac & Pradeep (2005) ($cm^{-1}$) | Assignment |
|---|---|---|
| 3109 | 3115 | $\nu$ (OH) |
| 3047 | 3045 | Crystal-split OH |
| 2954 | 2953 | $\nu$ (CH) |
| 2751 | 2755 | Crystal-split OH |
| 2581 | 2581 | Crystal-split OH |
| 1709 | 1708 | $\nu_s$(C=O) |
| 1390 | 1389 | $\delta$ (COH) |
| 1373 | 1373 | $\delta$ (HCO) |
| 1214 | 1213 | $\delta$ (C−O) |
| 1072 | 1072 | $\delta$ (CH) |
| 927 | 927 | $\delta$ (OH) |
| 710 | 711 | $\delta$ (OCO) |

It is known that in gas and liquid phases, formic acid exists in a dimer form because of hydrogen bonding. Features of the formic acid FTIR spectrum at 13 K are shown in Table 1. In this table, the first column lists the wavenumbers of the species found in the virgin ice spectrum, and the second column shows the wavenumbers found by Cyriac & Pradeep (2005), for comparison. The formic acid assignments are displayed in the last column. These features are compatible with the dimer features in the literature and are in concordance with Cyriac & Pradeep (2005), suggesting that in the solid state, the deposited molecules exist principally in the dimer form. Figs 2(a) and (b) present a comparison between the IR spectra of HCOOH ice at 13 K and the spectra taken at two different ion fluences ($1 \times 10^{12}$ and $1 \times 10^{13}$ ion $cm^{-2}$). The features have been identified following the work of Cyriac & Pradeep (2005). Formic acid dimer exhibits intense O–H stretching features, usually centred at 3000 $cm^{-1}$. The free hydroxyl stretching vibration (close to 3570 $cm^{-1}$), due to monomer, is not observed here.

The three peaks at 3047, 2751 and 2581 $cm^{-1}$ are a result of the three crystal-split components of the O–H stretching fundamental

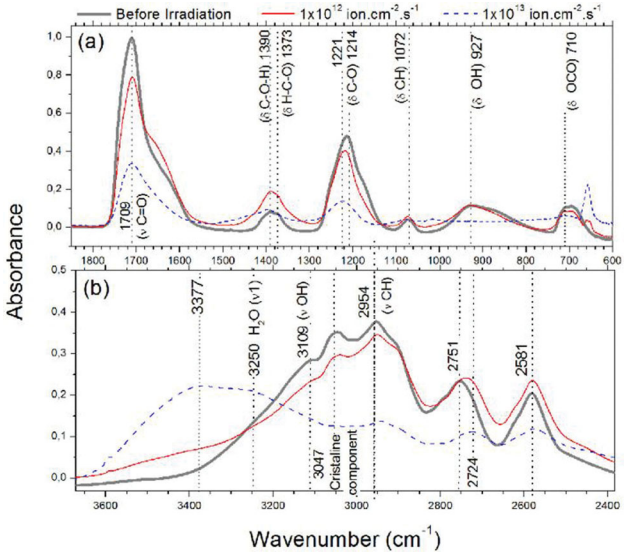


**Figure 2.** Experimental IR spectra of HCOOH at 13 K, before and after irradiation, in the (a) 1800–600 $cm^{-1}$ and (b) 3600–2400 $cm^{-1}$ ranges, respectively. The features have been assigned by using information from Cyriac et al. (2005).

(Cyriac & Pradeep 2005). The 3047 $cm^{-1}$ peak vanishes at high fluences. Thus, in the current experiment, the formic acid ice was formed initially in the dimer form, with a smaller fraction of the crystalline phase.

### 3.1 Column densities and cross-sections

The molecular column density ($N$, molecules $cm^{-2}$) of the sample was determined from the relation between absorbance $Abs_\nu = \log(I_0/I)$ and the IR absorption coefficient of the band (band strength). $A$-value (cm molecule$-1$) of the respective sample vibrational mode can be found in D'Hendecourt et al. 1986. In this expression, $I_0$ is the initial intensity of the irradiation beam at a specific frequency and $I$ is the intensity after passing through a sample. Tables 2 and 3 give the positions of the vibrational bands and their band strengths used in this work.

**Table 2.** Assignments, peak position and specific destruction cross-section for a vibration mode ($\sigma_{d,\nu}$) for the HCOOH bonds.

| Species | Position ($cm^{-1}$) | λ (μm) | $\sigma_{d,\nu}$ ($\times 10^{-13}$ $cm^2$) |
|---|---|---|---|
| δ (OCO) | 710 | 14.1 | (3.8 ± 0.5) |
| δ (OH) | 927 | 10.3 | (4.1 ± 0.3) |
| δ (CO) | 1214 | 8.2 | (1.3 ± 0.7) |
| $\nu_s$(C=O) | 1709 | 5.9 | (1.4 ± 0.3) |
| ν (OH) | 2581 | 3.9 | (0.9 ± 0.1) |
| ν (OH) | 2751 | 3.6 | (1.3 ± 0.7) |

The initial column density of the HCOOH ice ($N_0 = 3.21 \times 10^{18}$ molecules $cm^{-2}$) was determined from the integrated area of the band $\nu_s$(C=O) at 1709 $cm^{-1}$. Among all the observed bands, this shows the behaviour closest to an exponential decay. The values of the column density as a function of fluence $N(F)$ were obtained using the same procedure as in de Barros et al. (2011). Fig. 3(a) shows the $N(F)$ values for the different bonds of HCOOH as a function of the 267-MeV $Fe^{22+}$ beam fluence. The bands are related to the different vibration modes of each bond. All band areas are normalized at $F_c = 0.35 \times 10^{13}$ ions $cm^{-2}$ to the area of the 1709 $cm^{-1}$ band, which is intense and has the most reliable $A$-value because of its very small rising-up effect at the beginning of irradiation. The normalization at $F_c = 0.35 \times 10^{13}$ does not change the dissociation cross-section value, because this quantity depends on the relative exponential decay rate. The choice of this $F_c$ value comes from the fact that for $F < F_c$, the $N(F)$ slopes for the distinct HCOOH bands are different while, for $F > F_c$, the four slopes converge into values close to that of the 1709 $cm^{-1}$ band. As shown in Fig. 3(b) for each band, apparent variations of $N(F)$ with respect to an exponential decay appear in the region of low fluence. This behaviour is still under investigation and is expected to be a result of the variation of the $A$-value when changes of the crystalline phase and/or ice compaction occur. Because the determination of the destruction cross-section is based on the hypothesis that the variation of the column density $N(F)$ is proportional to $N(F)$ for any fluence $F$, which leads to equation (1), the fitting of a single exponential function should be performed accordingly. Data presented in Figs 3(a) and (b) indicate that compaction (or phase change) occurs at least up to $F^{max}$. Therefore, fitting must be carried out for $F > F_{max}$ (or even $F > F_c$ for some bands). Fig. 4 shows the $N_K$ dependence of HCOOH and its $k$ daughter species on the 267-MeV $Fe^{22+}$ beam fluence. In this figure, lines represent data fittings with equations (1) and (2), respectively.

#### 3.1.1 *Specific dissociation cross-sections*

Fig. 3 shows the evolution with beam fluence of six HCOOH bands (normalized to the 1709 $cm^{-1}$ band at $F_c = 3.5 \times 10^{12}$ ions $cm^{-2}$). The main features of data are the following.

**Table 3.** Formation ($\sigma_{f,k}$) and destruction ($\sigma_{d,k}$) cross-sections for the daughter species, using the HCOOH matrix values of $\sigma_{d,\nu}$ to fit the column density variations using $\sigma_{d,\nu} = 1.4 \times 10^{-13}$ $cm^2$.

| Species | Position ($cm^{-1}$) | λ (nm) | $A$-value ($\times 10^{-17}$) ($cm\ mol^{-1}$) | $\sigma_{f,k}$ ($\times 10^{-13}$ $cm^2$) | $\sigma_{d,k}$ ($\times 10^{-13}$ $cm^2$) |
|---|---|---|---|---|---|
| CO | 2139 | 4675.08 | 1.1[a] | (0.3 ± 0.03) | (2.1 ± 0.2) |
| $CO_2$ | 3703 | 2700.51 | 0.1[b] | (0.3 ± 0.01) | (2.3 ± 0.1) |
| $CO_2$ | 2345 | 4268.03 | 7.6, 21[c, d] | (0.3 ± 0.02) | (2.2 ± 0.2) |
| $H_2O$ | 3280 | 3048.78 | 20[e] | (0.4 ± 0.06) | (2.2 ± 0.3) |

[a] Jiang, Person & Brown (1975).
[b] Gerakines et al. (1995).
[c] Yamada & Person (1964).
[d] Sandford & Allamandola (1990).
[e] Allamandola, Sandford & Valero (1988).

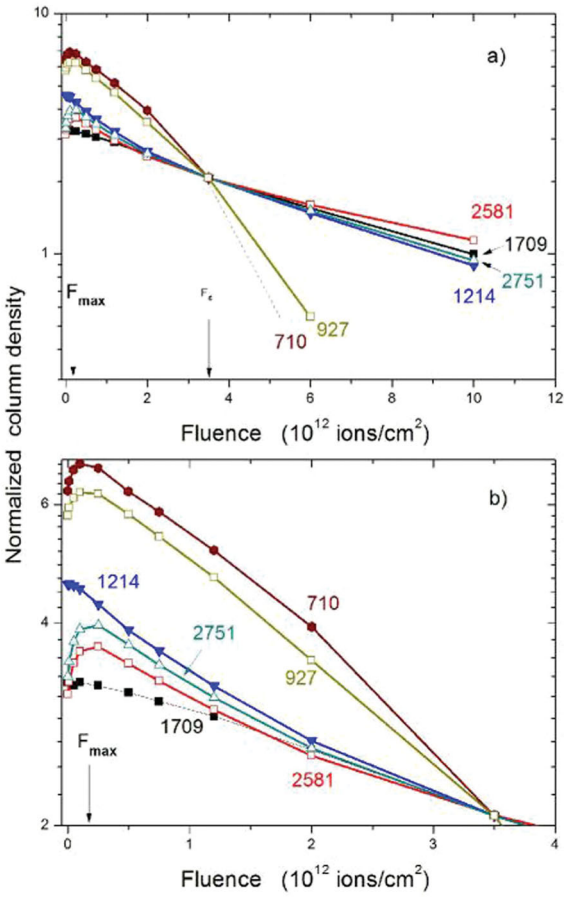


**Figure 3.** (a) Evolution of the molecular column density of HCOOH, as a function of the 267-MeV $Fe^{22+}$ beam, considering different vibration modes obtained in the IR spectra. (b) Expanded view (at low fluence region). The curves were normalized at a fluence of $3.5 \times 10^{12}$ cm$^{-2}$ to the value obtained from the 1709 cm$^{-1}$ band.

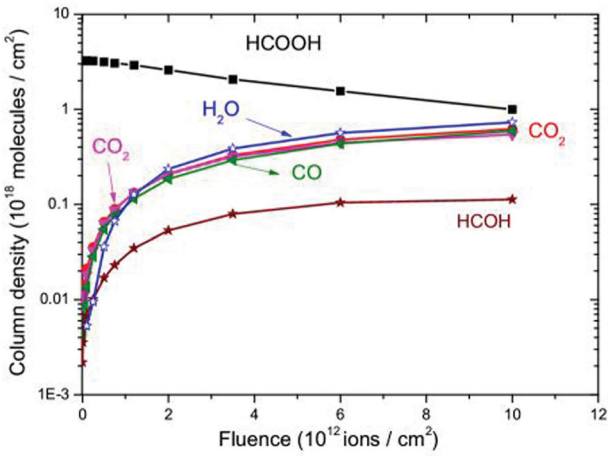


**Figure 4.** Column density dependence of HCOOH (considering the band 1709 cm$^{-1}$) and of the daughter species on the 267-MeV $Fe^{22+}$ beam fluence. The *A*-values are displayed in Tables 2 and 3. The solid lines are the data fittings.

(i) The column densities $N(F)$ of all bands present an apparent increase when the ice irradiation starts and they have a maximum value at $F_{max} \sim 0.2 \times 10^{12}$ ions cm$^{-2}$.

(ii) After $F_{max}$, the column density values decrease roughly exponentially and can be gathered into two groups: Group I, formed by the 1214, 1709, 2581 and 2751 cm$^{-1}$ bands, and Group II, formed by the 710 and 927 cm$^{-1}$ bands.

(iii) The column density values of Group I decrease with different slopes for $F_{max} < F < F_c$ and tend to have just one slope for $F > F_c$.

(iv) The column density values of Group II practically overlap with each other. For $F > F_c$, the analysis is not reliable because the baseline is difficult to determine.

The fact that the column densities seems to increase very fast at the beginning of irradiation (i.e. the up-rising effect) is attributed to ice compaction; during this process, the *A*-value of the IR absorption changes. It is conceivable – but not yet clear why – that the behaviour of $N(F)$ depends on the vibration mode of the sample molecules. Effects resulting from sputtering and molecular recombination are discussed in Section 4. At this time, we assume that the sputtering yield, $Y$, and the formation cross-section, $\sigma_f$, of the parent molecule are both negligible. To handle formally the distinct decay $N(F)$ of the vibration modes $\nu$, the specific destruction cross-section, $\sigma_{d,\nu}$, can be defined through the expression:

$$N_\nu(F) = N_{\nu,0} \exp(-\sigma_{d,\nu} F). \quad (1)$$

Here, $N_{\nu,0}$ is the predicted HCOOH column density at $F = 0$ (and not the experimental value of $N$ of the virgin ice). Fig. 3(a) shows that just after $F = F_{max}$, the lines corresponding to the 710, 927, 1214, 2751 and 2851 cm$^{-1}$ bands are practically parallel to each other, but change their slope after the end of compaction at $F = F_c$. In contrast, the values of the 1709 cm$^{-1}$ band decrease exponentially all the way; this is the reason for considering this line as a reference.

After fitting the data of the 1709 cm$^{-1}$ band over the whole fluence region with equation (1), the values of $\sigma_{d,\nu}$ have been determined; these are displayed in Table 2. For the other bands, the fittings were taken around the $F_c$ region. The dissociation cross-sections for Group I are around $1.3 \times 10^{-13}$ cm$^2$, while those for Group II are three times higher. These differences are compatible with the possibility of the destruction cross-section being different for distinct vibration modes. Such a behaviour is still under investigation.

### 3.1.2 *Formation cross-section*

The most abundant chemical species formed by Fe ion irradiation are CO, $CO_2$, $H_2O$, CO and $^{13}CO_2$. At 3563 cm$^{-1}$, there is a band that increases as the fluence increases, and this can be associated with the free hydroxyl group or with HCOH. Zins, Joshi & Krim (2011) have shown that the hydroxyl radical absorbs very close to this position, at around 3560 cm$^{-1}$, while Bennett et al. (2007) have identified this band as HCOH. The evolutions of their column densities as a function of fluence are presented in Fig. 4. At 1385 cm$^{-1}$, there is a band that could be a result of HCOOH itself or of $HCOO^-$ (Moore & Hudson 1998). Because this band increases as the fluence increases, it can be seen to be a result of the formation of $HCOO^-$ rather than of HCOOH.

According to de Barros et al. (2011a), if the products of the parent molecule $i = 1$ (with the index omitted hereafter for simplicity) are formed independently, as a function of the fluence, their column

densities can be written as

$$\frac{N_k(F)}{N_{\nu,0}} = \sigma_{\mathrm{f},k}\left(F - \frac{\sigma_{\mathrm{d},\nu}+\sigma_{\mathrm{d},k}}{2}F^2\right) = \sigma_{\mathrm{f},k}\left(F - \frac{1}{2}\sigma_{\mathrm{d},k}^{\mathrm{eff}}F^2\right). \quad (2)$$

Here, $\sigma_{\mathrm{f},k}$ is the formation cross-section of the $k$ species from HCOOH, $\sigma_{\mathrm{d},\nu}$ is the adequate destruction cross-section of the parent species and $\sigma_{\mathrm{d},k}$ is the destruction cross-section of the $k$ daughter species. The question is how to obtain $\sigma_{\mathrm{f},k}$ and $\sigma_{\mathrm{d},k}$ if the destruction cross-section of the parent molecule is not clearly determined. The column density slope near $F \sim 0$ does not depend on $\sigma_{\mathrm{d},\nu}$, so $\sigma_{\mathrm{f},k}$ can be determined by using the data only in this region. The fitting of $N_k(F)/N_{\nu,0}$ over a large fluence range is then reduced to just one parameter, which we call the effective destruction cross-section, $\sigma_{\mathrm{d}}^{\mathrm{eff}}$, defined as $\sigma_{\mathrm{d}}^{\mathrm{eff}} = (\sigma_{\mathrm{d},\nu} + \sigma_{\mathrm{d},k})$. Both quantities, $\sigma_{\mathrm{f},k}$ and $\sigma_{\mathrm{d}}^{\mathrm{eff}}$, can be determined unambiguously using equation (2), and the obtained values are presented in Table 3. The next step is to determine $\sigma_{\mathrm{d},k} = (\sigma_{\mathrm{f}}^{\mathrm{eff}} - \sigma_{\mathrm{d},\nu})$, which requires knowledge of the total destruction cross-section of the father molecule. As shown in the last column of Table 2, $\sigma_{\mathrm{d},k}$ has been calculated by considering $\sigma_{\mathrm{d},\nu} = 1.3 \times 10^{-13}$ cm$^2$.

### *3.1.3 Change of structure and band shift*

The positions of some bands, such as those at 1214 and 2751 cm$^{-1}$, change with the fluence. Fig. 5 shows the redshift dependence of these bands on the fluence. The OH feature of formic acid at 2751 cm$^{-1}$ is redshifted by ∼30 cm$^{-1}$. Slowly, the crystalline/amorphous fraction of the ice changes with the fluence, causing a variation in the corresponding $A$-value. Such behaviour occurs for most of the observed bands of formic acid and it explains the apparent and small column density increase at the beginning of irradiation (Fig. 3b). Note that such a change of morphology of the ice is accomplished in the low-fluence regime ($F < F_{\mathrm{c}}$). For higher fluences, no redshift is observed for the six measured band areas; all the column densities start to decay exponentially at the same rate. This phenomenon has been attributed to phase transition and/or ice compaction induced by UV or ion irradiation (e.g. Leto & Baratta 2003; Raut et al. 2007; de Barros et al. 2011).

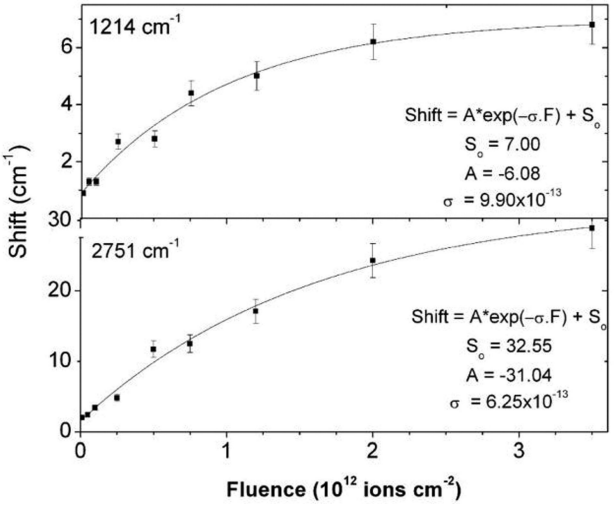


**Figure 5.** Variation of the peak centre of the 1214 and 2751 cm$^{-1}$ bands as a function of the ion fluence. The error bars are about 10 per cent.

These results can be explained as follows. (i) The IR peak shape is sensitive to changes in the ice structure. (ii) The $A$-value for virgin ice is not the same as for a high-fluence regime when the ice phase reaches equilibrium for irradiated material. (iii) The relative variations in the $A$-value for distinct IR bands of the same molecular species are different from each other in the low-fluence region.

### 3.2 Molecular half-life of formic acid in the interstellar medium and in the Solar system

Electron excitation is by far the most important process caused by the interaction between cosmic rays and matter. The ejected electron might have enough energy to further ionize and excite the neighbouring molecules, resulting in second-generation ions, radicals, electrons, photons and excited species. The secondary ions, formed by the impact, might participate in various ion–molecule reactions and might possibly be neutralized by secondary electrons to form reactive neutral species or stable molecules. The formed radicals might react with other radicals or molecules to form the final products. When the ionic projectiles pass through the target material, they continually transfer their energies to the ice molecules.

The 267-MeV Fe atoms have a velocity of around 3 cm ns$^{-1}$, corresponding to a few Bohr velocities ($v_{\mathrm{Bohr}} \sim 1$ cm ns$^{-1}$). For ion beams that have velocities near or above the Bohr velocity, the projectile energy and momentum are mainly transferred to the target by ion–electron interaction (i.e. the electronic stopping regime). The projectile traverses each molecular layer in $10^{-17}$ s, losing a small amount of its energy along the pathway, modifying its charge state and velocity in about $10^{-16}$–$10^{-15}$ s.

Based on experiments with methanol ice, de Barros et al. (2011) have proposed that the destruction cross-section of methanol by heavy ions follows a power law as a function of the electronic stopping power for the analysed precursor and daughter species, $\sigma_{\mathrm{d}} \sim S_{\mathrm{e}}^{3/2}$. The stopping power was calculated by using the SRIM code written by Ziegler, Biersack & Littmark (1985). Although the scattered points, de Barros et al. (2011) found $n = 1.5 \pm 0.5$, which turns out to be the same value we have obtained in the current work. This result confirms that the formation of new molecules is not very sensitive to most of the projectile and target parameters, because the destruction cross-section can be well described only as a function of the energy transferred to the solid per length unit. Godard et al. (2011) have suggested a power-law dependence $\sigma_{\mathrm{d}} \sim S_{\mathrm{e}}^{1.3}$ for the C–H destruction cross-section, in close agreement with the methanol results. Because there are no data available on the destruction cross-section for formic acid, the current data are fitted by the values of the expression, $\sigma_{\mathrm{d}} = aS_{\mathrm{e}}^{n}$, where the values $n = 0.5$, 1.0, 1.5 and 2.0 are assumed (Fig. 6). The fitting for $n = 0.5$ is not a good fit and it is not shown in Fig. 6. The factor $a$ was estimated using the $S_{\mathrm{e}}$ value for 267-MeV Fe ions in formic acid ice and the destruction cross-section $\sigma_{\mathrm{d},\nu}$ was estimated for the $\nu_{\mathrm{s}}(C=O)$ band, at 1709 cm$^{-1}$, found in this work (Table 2). This destruction cross-section provides the molecular half-life of formic acid in the region of study for the considered projectiles.

Fig. 7(a) shows the stopping power dependence on the projectile velocity (MeV per nucleon) for different cosmic ray constituents (H, He, C, O and Fe). The results have been obtained from the SRIM program. Fig. 7(b) shows how the destruction cross-sections ($\sigma_{\mathrm{d}}$) of these constituents depend on their energy/nucleon. The curves in Figs 7(a) and (b) have the same behaviour because we have considered $\sigma_{\mathrm{d}} = aS_{\mathrm{e}}^{3/2}$. The $a$-values are shown in Table 4. Fig. 7(c) exhibits the flux density ($\Phi_k$) for H, C, O and Fe, obtained from Shen et al. (2004). Note that hydrogen is the most

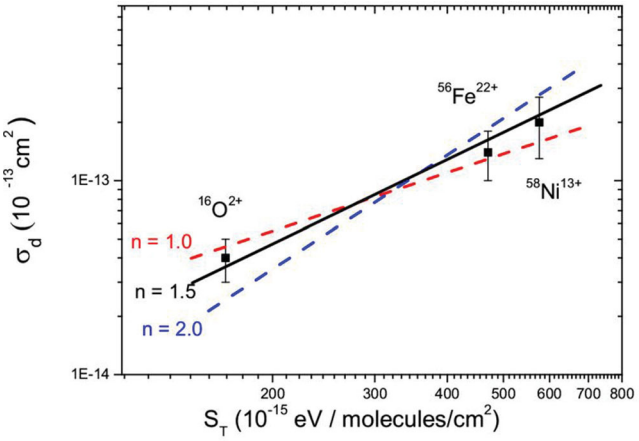


**Figure 6.** The dependence of the HCOOH destruction cross-section on the total stopping power. Data are for 6 MeV (O), 52 MeV (Ni; in preparation) and 267 MeV (Fe; the results of the current work). The lines correspond to the function $\sigma_d \sim S_e^n$, for $n = 3/2$ (solid line).

abundant cosmic ray constituent, but the Fe ions have the highest stopping power among the projectiles. In this way, the dissociation rate (Fig. 7d), defined as the product ($\Phi_k x \sigma_d$), is dominant for hydrogen at low velocities, but for Fe at high velocities. This is the reason why the Fe ions determine the half-life of frozen formic acid molecules in the ISM. In addition, it is important to point out the importance of the $n$-value in the law $\sigma_d = aS_e^n$. Table 5 shows that if $n = 0.5$, the hydrogen ions determine the formic acid half-life, while if $n = 1.5$, the formic acid is mainly destroyed by Fe ions.

The typical molecular half-lives ($\tau_{1/2}$) of HCOOH ice in the ISM are given by equation (3), where $\Phi_j$ is the estimated flux density of galactic cosmic rays, $\Phi_{HCR}(E)$, between $E$ and $E + dE$, and $\sigma_{d,k}$ is the destruction cross-section, which is a function of the ion energy to a given atom $j$:

$$\tau_{1/2} = \frac{\ln(2)}{\sum_j \int \Phi_j(E)\sigma_{d,j}(E)\,dE}; \quad (3)$$

$$\frac{dn}{dE} = \frac{CE^{0.3}}{(E + E0)^3}. \quad (4)$$

The sum $\sum_j \int \Phi_j(E)\sigma_{d,j}(E)\,dE$ must be performed over all galactic cosmic ray ions ($j$ = H, He, Li, Be, B, C, ...). Here, only H, He, C, O and Fe ions are considered.

The integral $\int \Phi_k(E)\sigma_{d,k}(E)\,dE$ must be performed over the whole energy range (i.e. over the area below the curve given in Fig. 7d).

Details of this calculation can be found in de Barros et al. (2011b). The galactic Fe flux was obtained from Shen et al. (2004), using the differential cosmic ray flux for Fe ions (equation 4), which is given in particles cm$^{-2}$ s$^{-1}$ sr$^{-1}$ (Mev per nucleon)$^{-1}$. In this equation, $C$ is a normalization constant ($C = 44$ for Fe) and $E_0$ is a parameter whose value is assumed to be 300 MeV. Webber & Yushak (1983) have shown that predictions using $E_0 = 400 \pm 100$ MeV can easily reproduce the measured $^3$He/$^4$He ratio and their observed spectra very well. Changes in $E_0$ modify substantially the spectra of low-energy cosmic rays, but they have almost no effect in the high-energy range.

Finally, the half-life of formic acid in the ISM, due to ion irradiation (Table 5), can be evaluated for the four selected values of the $n$ parameter, dividing ln (2) by the inverse of the anterior

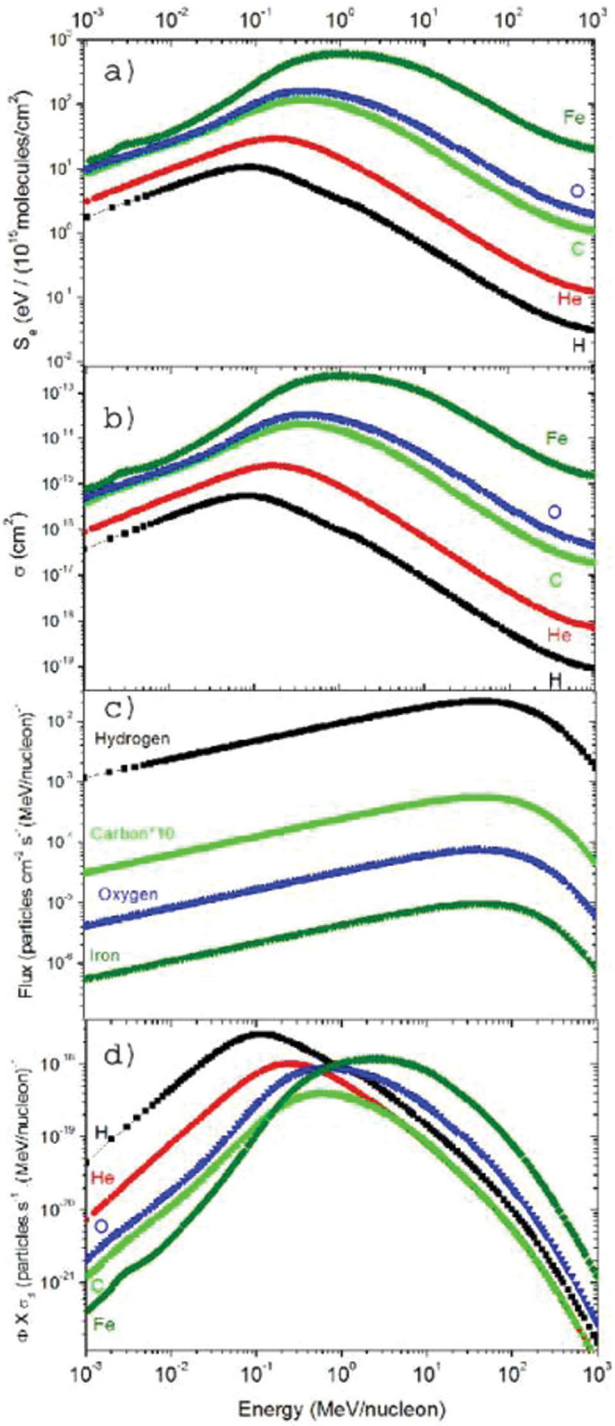


**Figure 7.** Energy per nucleon dependence of the main galactic cosmic rays relative to (a) the stopping power obtained from the SRIM program, (b) the destruction cross-section, $\sigma_d$, (c) the ISM flux density ($\Phi_k$) from Shen et al. (2004) and (d) the dissociation rate. In this calculation, we have considered only the $\sigma_d = aS_e^{1.5}$ dependence.

integral. Taking into account that the destruction by fast ions is an over-linear phenomenon as a function of the energy transferred to the solid (according to $\sigma_d = aS_e^n$ with $n = 0.5$, 1.0, 1.5 and 2.0), it is possible to calculate the formic acid half-life. Table 5 shows the formic acid half-life time in the ISM.

**Table 4.** The $a$-values corresponding to the four values of $n$ considered in the $\sigma_d = aS_e^n$ equation.

| $n$ | $a$-value [cm$^{-1}$ eV$^{-3/2}$ ($10^{15}$ molecules)$^{3/2}$] |
|---|---|
| 0.5 | $3.4 \times 10^{-15} \pm 1 \times 10^{-15}$ |
| 1.0 | $2.6 \times 10^{-16} \pm 4 \times 10^{-17}$ |
| 1.5 | $1.6 \times 10^{-17} \pm 2 \times 10^{-18}$ |
| 2.0 | $8.5 \times 10^{-17} \pm 4 \times 10^{-19}$ |

## 4 DISCUSSION

### 4.1 Penetration depth of light and heavy ions

In space, surfaces are constantly bombarded by light and heavy ions, which induce desorption and chemistry reactions. The ions have different penetration ranges, inducing chemical reactions at different layers. Remarkably, cosmic rays determine the secondary ions desorbed of the grains in the ISM, as well as in the atmospheres around comets and on planets. Thus, an understanding of the desorption processes can help us to understand the composition of atmospheres. Fig. 8 shows the penetration depth of some light and heavy ions inside formic acid ice, as predicted by the SRIM program, with density $\rho = 1.22$ g cm$^{-3}$. From Fig. 7(c), it can be seen that the particle flux is maximum for all constituents of cosmic rays at approximately 50 MeV per nucleon, making this range important from an astrophysical point of view. In this range, C, O and Fe ions have approximately the same penetration depth, of around 5 mm in HCOOH.

Fig. 8 also shows that typical galactic protons induce chemical reactions in ice layers that are much deeper than those processed by equivelocity Fe ions. Therefore, not only are Fe ions chemically more efficient than protons (even considering their flux ratio), but also the new molecular species formed by Fe are much closer to the ice surface and will be sputtered or sublimated first.

### 4.2 Ion desorption yield

In Section 3.1.1, we considered simplifications in order to obtain the HCOOH destruction cross-section directly from the data. The incident ion beam traversing the sample modifies the column density of the parent molecule ($N_\nu$) through three processes (i.e. molecular dissociation, sputtering and recombination):

$$\frac{dN_\nu(F)}{dF} = -\sigma_{d,\nu} N_\nu(F) - Y(F) + \sum_k \sigma_{f,k} N_k(F). \quad (5)$$

Here, $Y(F)$ is the sputtering yield of the parent molecule, $\sigma_{f,k}$ is the formation cross-section from the daughter species $k$ and $N_k(F)$ is the column density of this species at a fluence $F$. At the very beginning of irradiation, each projectile impacts in a virgin site of the sample and $Y(F)$ is equal to $Y_0$, the sputtering yield of the non-irradiated sample. After a large fluence $F$, projectile tracks overlap each other, the abundance of the parent molecule at the target surface has decreased and $Y(F) = [N_\nu(F)/N_{\nu,0}]Y_0$. Considering fluences that are not too high, $N_k(F) \ll N_\nu(F)$ and the recombination term can be neglected. Then, equation (5) becomes

$$\frac{dN_\nu(F)}{dF} = -\left(\sigma_{d,\nu} + \frac{Y_0}{N_{\nu,0}}\right) N_\nu(F), \quad (6)$$

whose solution is

$$N_\nu(F) = N_{\nu,0} \exp(-\sigma'_{d,\nu} F). \quad (7)$$

Here, $\sigma'_{d,\nu} = \sigma_{d,\nu} + Y_0/N_{\nu,0}$ is a total destruction cross-section, which includes the dissociation and sputtering processes. In fact, the values presented in Table 2 correspond to $\sigma'_{d,\nu}$; accordingly, $\sigma_{d,\nu}$ should be determined by $\sigma'_{d,\nu} - Y_0/N_{\nu,0}$. Because $\sigma'_{d,\nu} \sim 10^{-13}$ cm$^2$ and $N_{\nu,0} \sim 3 \times 10^{18}$ molecule cm$^2$, we have $\sigma'_{d,\nu} N_{\nu,0} \sim 3 \times 10^5$ molecules per impact as a sputtering yield value, below which $\sigma_{d,\nu} \sim \sigma'_{d,\nu}$.

The ion sputtering yield for heavy ion bombardment of HCOOH at MeV energies is shown to be ~1 ion per impact, but neutral emission is known to be many orders of magnitude higher. Another relevant aspect to be considered in the $Y_0$ evaluation is the existence of residual gas layering during irradiation, which might prevent HCOOH sputtering. The usual candidates are $N_2$, $O_2$ and $H_2O$. Unfortunately, $N_2$ and $O_2$ absorption are very difficult to observe using the FTIR technique, and $H_2O$ is one of the main daughter molecules of HCOOH. The $N_k(F)$ evolution for $H_2O$, depicted in Fig. 4, is quite well fitted by equation (2). Relatively small OH

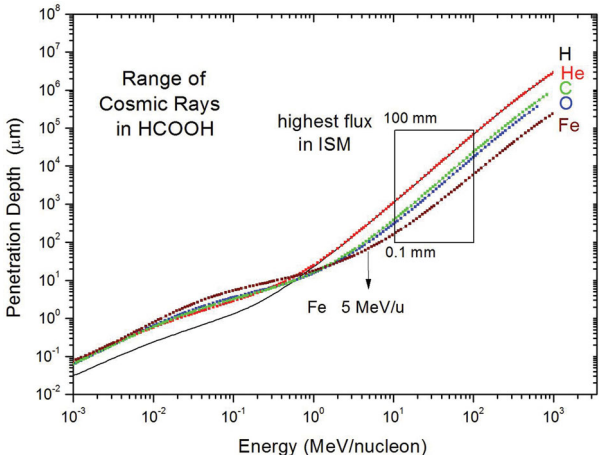


**Figure 8.** Perpendicular penetration of H, He, C, O and Fe projectiles in formic acid ice as predicted by SRIM. Because the maximum fluxes for all these ions occur in the 10–100 MeV $u^{-1}$ region (Fig. 7 c), typical value for Fe penetration in this ice cover 0.1–10 mm, while the ranges for He and H are 1–100 mm.

**Table 5.** Predictions for $t_{1/2}$ of formic acid bombarded by H, He, O, C and Fe ions, corresponding to the four values of $n$ in the $\sigma_d = aS_e^n$ equation.

| $n$ | H (Ma) | He (Ma) | C (Ma) | O (Ma) | Fe (Ma) | Total (Ma) | Total (s) |
|---|---|---|---|---|---|---|---|
| 0.5 | 2.6 | 20.7 | 184 | 101 | 242 | 2.2 | $6.9\times 10^{13}$ |
| 1.0 | 95 | $3.6 \times 10^2$ | $1.1 \times 10^3$ | 432 | 361 | 52 | $1.6 \times 10^{15}$ |
| 1.5 | $2.5 \times 10^3$ | $4.6 \times 10^3$ | $5.3 \times 10^3$ | $1.7 \times 10^3$ | 540 | 307 | $9.7 \times 10^{15}$ |
| 2.0 | $4.4 \times 10^4$ | $4.2 \times 10^4$ | $2.0 \times 10^4$ | $5.4 \times 10^3$ | 755 | 623 | $1.7 \times 10^{16}$ |

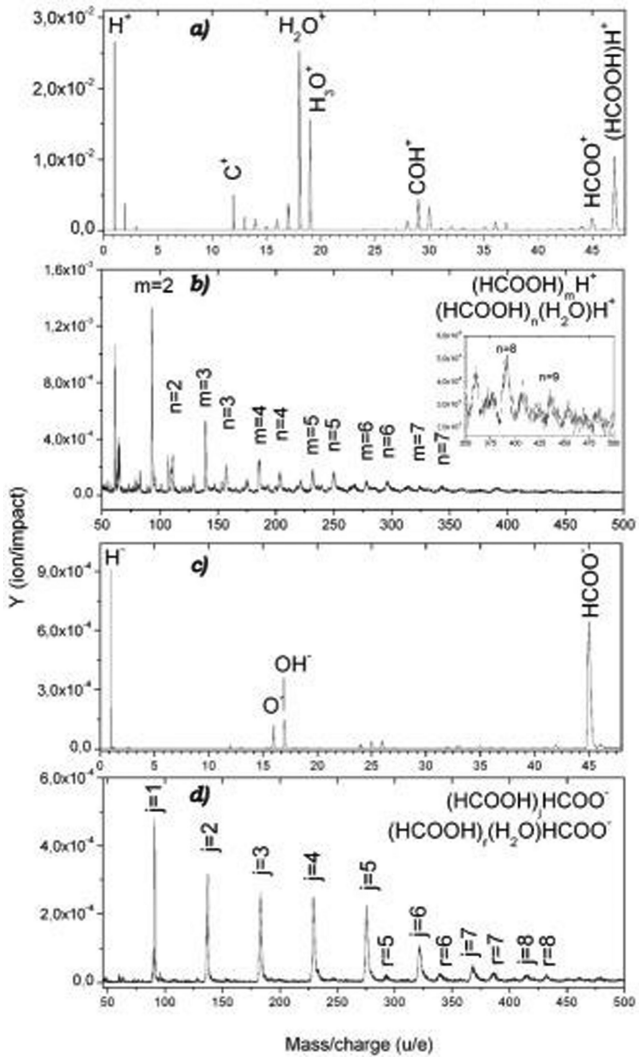


**Figure 9.** Mass spectra for formic acid ice at 56 K obtained by PDMS: (a) low-mass/charge and (b) high-mass/charge positive fragments; (c) low-mass/charge and (d) high-mass/charge negative fragments (adapted from Andrade et al. 2008).

dangling bonds lines have been found in the current measurements, indicating the presence of (at least some) amorphous water superficial layers. However, the main argument to assume that $Y(F)$ is negligible for the current analysis is that water layering has been detected in similar experiments with the same experimental set-up. In this sense, the values presented in Table 2 are correct. Finally, Fig. 3(b) reveals that the data points of the Group I lines tend to be higher than the exponential decay behaviour, an indication of the recombination effect described by equation (5). The change in the slope of the $N(F)$ decay at $F = F_c$ is not completely clear, but has been attributed to sample compaction (see Palumbo, Baratta & Spinella 2006) for ices or to polymerization of solid targets at room temperature (see Ferreira-Rodrigues et al. 2011).

### 4.3 Dissociation and chemical reactions

For a better understanding of the fast and slow physical–chemical process related to the radiation-induced dissociation of formic acid, mass spectrometry data, taken from Andrade et al. (2008), have been analysed to complement the current FTIR results. Fig. 9 represents the break-up of the formic acid ice into molecular fragments and cluster ions (adapted from Andrade et al. 2008). Figs 9(a)–(d) show the low- and high-mass/charge positive ions and the low- and high-mass/charge negative ions, respectively. These have desorbed because of the fission fragments of californium ($^{252}$Cf) bombardment on formic acid ice at 56 K. Details can be seen in Andrade et al. (2008), where plasma desorption mass spectrometry (PDMS) has been used to simulate the effects of energetic charged particles (e.g. cosmic rays) on interstellar/cometary ices. The prediction is that the most intense clusters in the positive spectrum are $(HCOOH)_mH^+$, with $1 \leq m \leq 7$ and $(HCOOH)_nH_3O^+$ – or $(HCOOH)_n(H_2O)H^+$ – with $1 \leq n \leq 8$. As seen in the negative ion spectrum, the most intense clusters are $(HCOOH)_jCOOH^-$, with $1 \leq j \leq 9$, and $(HCOOH)_rOH^-$, with $4 \leq r \leq 10$.

From the integrated area of the positive ion PDMS spectrum in the low-mass region, $1 \leq m/q \leq 45$, the desorption rate ($Y_{\text{ion-low}}$) of $2.9 \times 10^{-1}$ ions per impact is determined, while the desorption rate for the $(HCOOH)H^+$ ion is [$Y_{(HCOOH)H+} = 2.1 \times 10^{-2}$] ions per impact. The integrated spectrum in the high-mass/charge ($m/q >$ 47 u/$e$ region) is formed mainly by peaks resulting from the cluster series from which the desorption yield ($Y_{\text{ion-high}}$) of $2.2 \times 10^{-1}$ ions per impact is calculated. In the case of positive ions, the formation of positive fragments is slightly more intense than the formation of positive clusters.

The integrated negative ion PDMS spectrum in the low-mass/charge region, $1 \leq m/q \leq 44$ u/$e$, shows a desorption rate ($Y_{\text{ion-low}}$) equal to $6.8 \times 10^{-3}$ desorbed ions per impact. This value is almost the same as the desorption rate of the $HCOO^-$ ion, which is $Y_{HCOO-} = 5.6 \times 10^{-3}$ desorbed ions per impact. The negative ion integrated spectrum in the high-mass/charge ($m/q >$ 45 u/$e$) region, which includes mainly the cluster series, shows a desorption yield ($Y_{\text{ion-high}}$) of $7.8 \times 10^{-2}$, which is one order of magnitude higher than in the low $m/q$ region.

These results reveal that the bombardment of heavy ion cosmic rays desorbs approximately 0.6 ions per impact, of which 0.5 are cations and 0.1 are anions. Considering that the sputtering yield is $1 \times 10^3$, the ratio ion/neutral of the emitted particles is $\sim 6 \times 10^{-4}$. Because the cations are more easily desorbed (the ratio cation/anion $\sim$5), electron emission must occur, otherwise the grain in the ISM becomes negatively charged.

Table 6 shows the yield ratios among the desorbed ions. In this table, PTIY is the total number of positive ions and NTIY is the total number of negative ions desorbed from formic acid ice under $^{252}$Cf FF bombardment. In both cases, the spectra are integrated over the 1–500 u/$e$ range. PTFY is the desorption rate of low-mass ions, in the 1–46 u/$e$ range, and NTFY is the desorption rate to low-mass ions, integrated from negative spectra in the 1–45 u/$e$ range. PTCY and NTCY are the desorption rates of positive and negative total cluster ions, which have $47 \leq m/q \leq 500$ u/$e$. NT($HCOO^-$)Y is the total desorption rate of negative ions with $HCOO^-$ attached or the $HCOO^-$ ion, while NTFY* is the desorption rate of negative fragments different from $HCOO^-$ and their clusters. PNTCY is the desorption rate of all clusters, for positive and negative ions, and PNTFY is the desorption rate of all fragments of positive and negative ions.

It is worth mentioning that $H_2O^+$ and $H_3O^+$ are observed to be two intense peaks in the positive ion PDMS spectrum (Andrade et al. 2008) and that the formation of $H_2O$ is also observed in the FTIR spectra after Fe bombardment (Ferreira-Rodrigues et al. 2011). This ion can be formed from dissociation of $(HCOOH)_n(H_2O)HCOO^-$, but it can also be formed from formic acid ice irradiated with soft X-ray photons (Andrade et al. 2009). Boechat-Roberty et al. (2005)

**Table 6.** Desorption yield ratio for positive and negative fragments and cluster ions. PTIY is the total number of positive ions and NTIY is the total number of negative ions desorbed from formic acid ice under bombardment of $^{252}$Cf FF. PTFY and NTFY are the positive and negative ion desorption yields, respectively, for low-mass ions. PTCY and NTCY are the desorption yields for positive and negative total cluster ions, respectively. NT($HCOO^-$)Y is the total desorption yield for negative ions with $HCOO^-$ attached or the $HCOO^-$ ion, while NTFY* is the desorption yield to negative fragments different from $HCOO^-$ and their clusters. PNTCY is the desorption yield of all clusters, positives and negatives, and PNTFY is the desorption yield of all fragments, positives and negatives.

| | |
|---|---|
| PTIY/NTIY | 5.0 |
| PTCY/NTCY | 3.1 |
| PTFY/NTFY | 23.0 |
| PTFY/PTCY | 1.2 |
| NTFY/NTCY | 0.16 |
| NT($COOH^-$)Y/NTFY* | 12.3 |
| PNTCY/PNTFY | 1.05 |

have shown that in the gas phase, this ion is also formed because of the impact of soft X-rays (at 300 eV), but with low intensity, suggesting that in condensed phase its formation is more efficient.

The formic acid cation $HCOOH^+$ is not observed directly in the ISM. Even though the decomposition products of HCOOH, such as $HCOO^+$ and $HCO^+$, have been observed by radio telescopes (Hakobian & Crutcher 2012). These species play an important role in molecule formation in the ISM, probably because of the low formation of the formic acid cation $HCOOH^+$, as seen in our present data. Electron loss or capture seems to be an inefficient process for formic acid, which seems to prefer to receive a proton than to lose or capture an electron. $HCOOH^-$ also has a low probability of being formed, as shown in Fig. 9. Martin et al. (2005) did not observe these ions in electron capture by single formic acid, but they did see them as a product of the electron capture of its clusters. Fig. 10 shows a proposed scheme to form the observed products following heavy and energetic ions irradiation of pure formic acid ice.

As far as we know, there is no evidence that pure HCOOH ice is present in the ISM or in Solar System ices. Nevertheless, evidence has been found of a low formic acid abundance [HCOOH]/[$H_2O$] ratio in comets, lower than 0.1 per cent at 1 au from the Sun (Bockeleé-Morvan et al. 2000). This finding indicates that formic acid ice that exists in comets is mixed with other molecules, such as $H_2O$, CO and $CO_2$, which are the same molecules observed in our results.

An important argument for studying cosmic ray interaction with pure ices is based on methodology. Once these effects have been established, then ice mixtures should be considered in future experiments. The mixture of ices not only generates a larger number of formed species but also introduces new effects on the dissociation of molecules because of the modification in their chemical environment.

Because the number of ions desorbed from ice is low when compared to that of neutral species ($Y_{ion}/Y_{neutral} \sim 6 \times 10^{-4}$), it is usually difficult to detect ion signatures by radio telescope. However, as shown in this section, the ionic species formed from ion impacts on the ice are important from a chemical point of view, because they are much more reactive than neutral species.

## 5 REMARKS AND CONCLUSIONS

Formic acid ice at 15 K was irradiated by 267-MeV $^{56}Fe^{22+}$; its column density decrease was followed through mid-range IR vibration bands. The value of $1.4 \times 10^{-13}$ cm$^2$ has been found for the corresponding destruction cross-section. However, a value three times higher is obtained when the 710, $\delta$ (OCO), and 927 cm$^{-1}$, $\delta$ (OH), bands are analysed. The reason for this discrepancy is not clear, but it could be that crystallization and/or ice compaction are affecting the IR absorbance of each molecular vibration mode in different ways. In this way, we have introduced the concept of the specific dissociation cross-section, which depends on the vibration mode. We have also correlated the shift peaks with the dissociation (or destruction) of bonds and a cross-section is extracted from the shift.

In order to estimate the maximum molecular half-life of formic acid in the ISM and in the Solar System, we have studied the dissociation cross-section, considering only the C = O vibration mode. To predict the half-life of formic acid due to H, He, C, O and Fe ions, we have considered that the destruction cross-section follows a power law as a function of the electronic stopping power. For the analysed precursor, the relation $\sigma_{dv} \sim S_e^n$ was used for four values of $n$ (i.e. 0.5, 1.0, 3/2 and 2.0). A typical half-life for HCOOH ice in the ISM is predicted to be of the order of $10^6$–$10^8$ yr. If

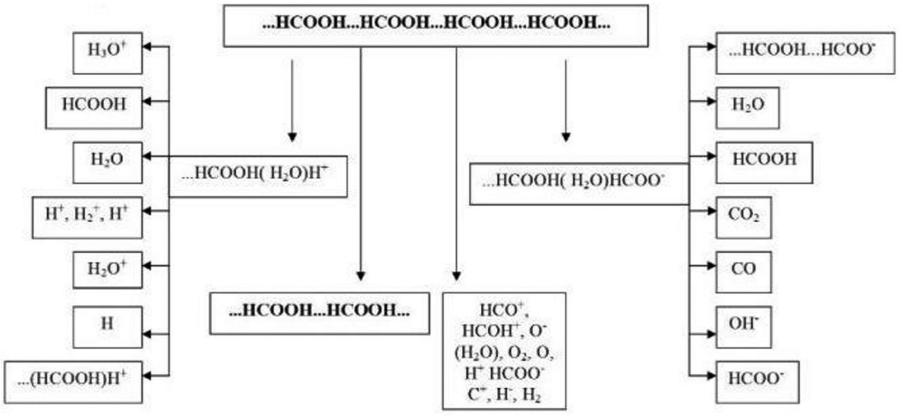


**Figure 10.** Proposed diagram for the dissociation of frozen HCOOH and for the successive chemical reactions induced by heavy and energetic ions.

$n = 3/2$ is selected, then the Fe ions determine the half-life of formic acid in the ISM.

In addition, it is shown that typical galactic light ions (H and He) induce chemical reactions in ice layers, which are much deeper than those processed by equivelocity heavy ions (C, Fe/Ni). This fact reinforces the necessity to take heavy cosmic ray effects into account in astrochemical models. In particular, it should be stressed that Fe ions are crucial in the production and ejection of new molecular species into space for two reasons: (i) heavy ions induce chemical reactions much more efficiently than protons in their respective highest flux region; (ii) Fe ions process the ice only near its surface, while protons do the same over a much larger range. This fact is especially relevant for large icy objects, because the surface material is the one sputtered and/or sublimated first. For clouds, this means that only the peripheral regions are processed by both light and heavy ion cosmic rays.

## ACKNOWLEDGMENTS

This work was supported by the region of Basse-Normandie (France) and by the French-Brazilian exchange programme CAPES-COFECUB. It is a pleasure to thank Th. Been and J. M. Ramillon for technical support. The experiment was performed at the GANIL facility in Caen, France. The Brazilian agencies CNPq (INEspaço) and FAPERJ also provided partial support.

## REFERENCES

Allamandola L. J., Sandford S. A., Valero G. J., 1988, Icarus, 76, 225
Andrade D. P. P., Rocco M. L. M., Boechat-Roberty H. M., Iza P., Martinez R., Homem M. G. P., da Silveira E. F., 2007, J. Elect. Spectr. Relat. Phenom., 155, 124
Andrade D. P. P. et al., 2008, J. Phys. Chem. C, 112, 11954
Andrade D. P. P., Boechat-Roberty H. M., Pilling S., da Silveira E. F., Rocco M. L. M., 2009, Surf. Sci., 603, 3301
Bennett C. J., Chen S. H., Sun B. J., Chang A. H. H., Kaiser R. I., 2007, AJ, 660, 1588
Bertie J. E., Michaelian K. H., Eysel H. H., Hager D., 1986, J. Chem. Phys., 85, 4779
Bockeleé-Morvan D. et al., 2000, A&A, 353, 1101
Boechat-Roberty H. M., Pilling S., Santos A. C. F., 2005, A&A, 438, 915
Briscoe J. F., Moore C. B., 1993, Meteoritics, 28, 330
Crovisier J., Bockeleé-Morvan D., Colom P., Biver N., Despois D., Lis D. C., 2004, A&A, 418, 1141
Cyriac J., Pradeep T., 2005, Chem. Phys. Lett., 402, 116
D'Hendecourt L. B., Allamandola L. J., Grim R. J. A., Greenberg J. M., 1986, A&A, 158, 119
de Barros A. L. F., Bordalo V., Seperuelo Duarte E., da Silveira E. F., Domaracka A., Rothard H., Boduch P., 2011a, A&A, 531, 15
de Barros A. L. F., Doramacka A., Andrade D. P. P., Boduch P., Rothard H., da Silveira E. F., 2011b, MNRAS, 418, 1363
Ehrenfreund P. E., Charnley S., 2000, ARA&A, 38, 427
Ehrenfreund P., Schutte W. A., 2000, Adv. Space Res., 25, 2177
Ferreira-Rodrigues A. M., Homem M. G. P., Naves de Brito A., Ponciano C. R., da Silveira E. F., 2011, Int. J. Mass Spectrom., 306, 77
Gerakines P. A., Schutte W. A., Greenberg J. M., van Dishoeck E. F., 1995, A&A, 296, 810
Godard M. et al., 2011, A&A, 529, A146
Guillemin R., Stolte W. C., Lindle D. L., 2009, J. Phys. B: At. Mol. Opt. Phys., 42, 125101
Hakobian N. S., Crutcher R. M., 2012, ApJ, 758, L18
Jiang G. J., Person W. B., Brown K. G., 1975, J. Chem. Phys., 64, 120
Leach S., Schwell M., Dulieu F., Chotin J. L., Jochimsb H. W., Baumgärtelb H., 2002, Phys. Chem. Chem. Phys., 4, 5025
Leto G., Baratta G. A., 2003, A&A, 397, 7
Liu S. Y., Girard J. M., Remijan A., Snyder L. E., 2002, ApJ, 576, 255
Maçôas E. M. S., Lundell J., Pettersson M., Khriachtchev L., Fausto R., Rasanen M., 2003, J. Mol. Spectrosc., 219, 70
Maréchal Y., 1987, J. Chem. Phys., 87, 6344
Martin I., Skalicky T., Langer J., Abdoul-Carime H., Karwasz G., Illenberger E., Stanob M., Matejcik S., 2005, Phys. Chem. Chem. Phys., 7, 2212
Martin I., Bertin M., Domaracka A., Azria R., Illenberger E., Lafosse A., 2008, Int. J. Mass Spectrom., 277, 262
Millikan R. C., Pitzer K. S., 1957, J. Chem. Phys., 27, 1305
Millikan R. C., Pitzer K. S., 1958, J. Amer. Chem. Soc., 81, 3515
Moore M. H., Hudson R. L., 1998, Icarus, 135, 518
Palumbo M. E., Baratta G. A., Spinella F., 2006, Mem. Soc. Astron. Ital. Suppl., 9, 192
Pilling S., Santos A. C. F., Boechat-Roberty H. M., de Souza G. G. B., Santanna M. M., Barros A. L. F., Wolff W., de Castro Faria N. V., 2006a, Brazilian J. Phys., 36, 538
Pilling S., Santos A. C. F., Wolff W., Santanna M. M., Barros A. L. F., de Souza G. G. B., de Castro Faria N. V., Boechat-Roberty H. M., 2006b, MNRAS, 372, 1379
Pilling S., Baptista L., Boechat-Roberty H. M., Andrade D. P. P., 2011a, Astrobiology, 11, 883
Pilling S., Duarte E. S., Domaracka A., Rothard H., Boduch P., da Silveira E. F., 2011b, Phys. Chem. Chem. Phys., 13, 15 755
Raut U., Famá M., Teolis B. D., Baragiola R. A., 2007, J. Chem. Phys., 127, 204713
Reva I. D., Plokhotnichenko A. M., Radchenko E. D., Sheina G. G., Blagoi Y. P., 1994, Spectrochim. Acta, 50A, 1107
Sandford S. A., Allamandola L. J., 1990, ApJ, 355, 35
Schutte W. A. et al., 1996, A&A, 315, L333
Seperuelo Duarte E., Boduch P., Rothard H., Been T., Dartois E., Farenzena L. S., da Silveira E. F., 2009, A&A, 502, 599
Shen C. J., Greenberg J. M., Schutte W. A., van Dishoeck E. F., 2004, A&A, 415, 203
Webber W. R., Yushak S. M., 1983, ApJ, 275, 391
Yamada H., Person W. B., 1964, J. Chem. Phys., 41, 2478
Ziegler J. F., Biersack J. P., Littmark U., 1985, The Stopping and Range of Ions in Solids. Pergamon, New York
Zins E. L., Joshi P. R., Krim L., 2011, MNRAS, 415, 3107

This paper has been typeset from a TEX/LATEX file prepared by the author.